Lab on a Chip

Accepted Manuscript

ROYAL SOCIETY OF CHEMISTRY

www.rsc.org/loc

We present a low-cost Lab-on-a-Chip option for cheap HIV diagnostics using whole blood, operating largely instrument-free, with rapid time-to-answer.

Journal Name

RSCPublishing

ARTICLE

Rapid, Low-Cost and Instrument-Free CD4+ Cell Counting for HIV Diagnostics in Resource-Poor Settings

Cite this: DOI: 10.1039/x0xx00000x

Received 00th January 2012,
Accepted 00th January 2012

DOI: 10.1039/x0xx00000x

www.rsc.org/

Macdara Glynn, David J. Kinahan and Jens Ducrée

We present a novel, user-friendly and widely autonomous point-of-care diagnostic to enable HIV monitoring in resource-poor regions where the current pandemic is most prevalent. To specifically isolate magnetically tagged CD4+ cells directly from patient blood, the low-cost and disposable microfluidic chip operates by dual-force CD4+ cell magnetophoresis; whereby the interplay of centrifugal- and magnetic fields govern the trajectory of target cells depending on whether the cell binds to a magnetic microbead. Instrument-free pumping is implemented by a finger-actuated elastic membrane; tagged beads are laterally deflected by a small and re-useable permanent magnet. The single-depth and monolithic microfluidic structure can easily be fabricated in a single casting step. After their magnetophoretic isolation from whole blood, estimation of CD4+ cell concentrations is then measured by bright-field inspection of the capture chamber. In addition, an optional fluorescence measurement can be used for confirmation of the bright-field result if required. On-chip CD4+ estimation produces a linear response over the full range of medically relevant CD4+ cell concentrations. Our technology combines high-efficiency capture (93.0 ± 3.3%) and cell enumeration.

Keywords: HIV Diagnostics, Point-of-Care, Resource-Poor Diagnostics, Microfluidics

Introduction

Since its initial identification and characterisation in the early 1980s [1, 2], HIV (human immunodeficiency virus) infection and the associated pathology of AIDS (acquired immunodeficiency syndrome) remain as an ongoing global pandemic disease. The most recent UNAIDS report estimates that over 35 million people were living with HIV in 2012, with total estimated deaths since the emergence of the disease of around 36 million [3]. This places HIV as one of the primary infectious diseases of the modern age. Encouragingly, at a global level there is a year-on-year decrease in the overall number of new HIV infections (since 1996) and deaths (since 2005), even though the overall number of people living with HIV is increasing; this is due, at least in part, to increasing access to anti-retroviral therapies (ART) which significantly extend the (average) life expectancy of patients [4]. Although encouraging, 2012 statistics also showed that 71% of those living with HIV, and 75% of the AIDS-related deaths occurred in Sub-Saharan Africa [3]. These statistics clearly underpin that resource should primarily be concentrated at this large reservoir of HIV.

The HIV Treatment Cascade (sometimes called the HIV/AIDS Care Continuum) is a public health tool a HIV-infected individual must follow to achieve viral suppression [5, 6]. The first step in this cascade (after infection) is diagnosis, often referred to as "aware of status". This is followed by: link to medical care, continuation of medical care, ART, and finally, viral suppression. In 2012, only 51% of those living with HIV were aware of their status in Sub-Saharan Africa, and in some countries (i.e. Burkina Faso), as little as 10% of infected individuals are likely to be aware of their status [3]. A primary reason for this shortfall in diagnosis is the technical challenge of delivering effective testing to populations in such resource-poor regions. Often, HIV diagnostics in these areas is attempted using technology more applicable to high-income and infrastructure-advanced regions – such as clinical flow cytometry at a central national facility. This strategy coincides with a high level of patients dropping out of treatment regimens – known as "loss to follow up" [7, 8].

Compact "Point-of-Care" (PoC) technologies which can be taken along by medical staff to patients and set up in mobile clinics distant from urban centres are frequently deemed a more promising approach [9]. Indeed, a study by Jani *et al*. showed that loss to follow up dropped from 64% to 33% at a test clinic in Mozambique following introduction of PoC testing [10]. There

are a number of such PoC instruments specifically designed for HIV testing in resource-poor countries on the market, and more in the late stages of validation before commercial release as recently reviewed [11].

A reliable measure of HIV infection is the concentration of CD4-expressing T-helper cells (Th-cells) in the blood of a patient. As the target of the HIV virus, a reduction in the number of these cells can diagnose and / or stage the infection. The number of CD4+ cells in a healthy individual will vary depending on a variety of demographic, environmental and genetic factors [12], but in general a healthy number of CD4+ cells is greater than 1200 cells / µl of whole blood, and can range as high as 2072 cells / µl [13]; regardless, the current threshold for initiation of ART since 2013 is 500 cells / µl [3].

We present here a HIV test which determines the number of CD4+ cells from a small volume of whole blood loaded to a readily manufacturable and simple-to-operate microfluidic chip. Although blood-based CD4+ cellular estimation is common in many of the devices [11], the presented strategy can be devised instrument-free as the flow is driven by mere finger-actuation. Furthermore, the single-depth microfluidic features can be monolithically manufactured, for example by casting, hot embossing or injection moulding, without the need for hybrid integration of functional materials, e.g. for pumping and valving. This clearly distinguishes our work from other finger-actuated micro-devices which require more complex and thus (potentially) more costly and error-prone concepts of flow control: using a ball to deform a barrier film [14], installing a multi-part pumping structure cast independently of the final chip [15-17], or controlling fluidic passage using valving [18].

Isolation of cells based on expression of a specific protein marker binding to magnetic beads (magnetophoresis) has been demonstrated. Published and commercial applications of magnetophoresis can, however, often involve complex design as the second force that acts in a distinct direction to the magnetic force can require peripherals with active components, electronics and software. Such peripherals include syringe pumps [19, 20], or more recently, a centrifuge [21]; hence compromising cost efficiency and ease of deployment of such a device in infrastructure- and expertise-poor regions.

Similarly, current detection strategies, such as the two currently available commercial PoC devices (Alere Pima™ and Partec CyFlow® miniPOC), frequently involve complex instrumentation, e.g. direct fluorescence measurement [11] using antibodies specific to CD4+ cells [22-25]. The use of such specialised fluorescent antibodies can be both a cost and storage burden. Other methods to enumerate isolated CD4+ cells include electrical impedance measurement [26-28], and surface plasmon resonance (SPR) [29] – both of which are associated with technically advanced and intricate hardware. Lens-less electronic CCD detection [30] can provide a simpler instrumentation platform for CD4+ enumeration.

We present the described microfluidic chip, as an option to integrate specific, dual-force (fluidic and magnetic) CD4+ cell isolation from whole blood, with a highly simplistic optical readout using only a bright-field magnification option – such as a common microscope. A more sensitive readout can also be achieved using optional UV-based imaging, but without the need for an antibody binding step.

Operational Principle

A pneumatic fluidic reservoir (P1) at the base of the chip connects directly to the separation chamber (Fig. 1ii) and a secondary reservoir (P2) located at the opposite end of the separation channel. The sample input port is positioned directly below P2. Midway down the separation channel is the CD4+ capture locus. A permanent magnet is placed perpendicular to the pneumatically-driven flow of liquid. Prior to testing, the chip is primed by a degas-driven flow procedure (see Section "Chip Fabrication and Priming") with liquid buffer.

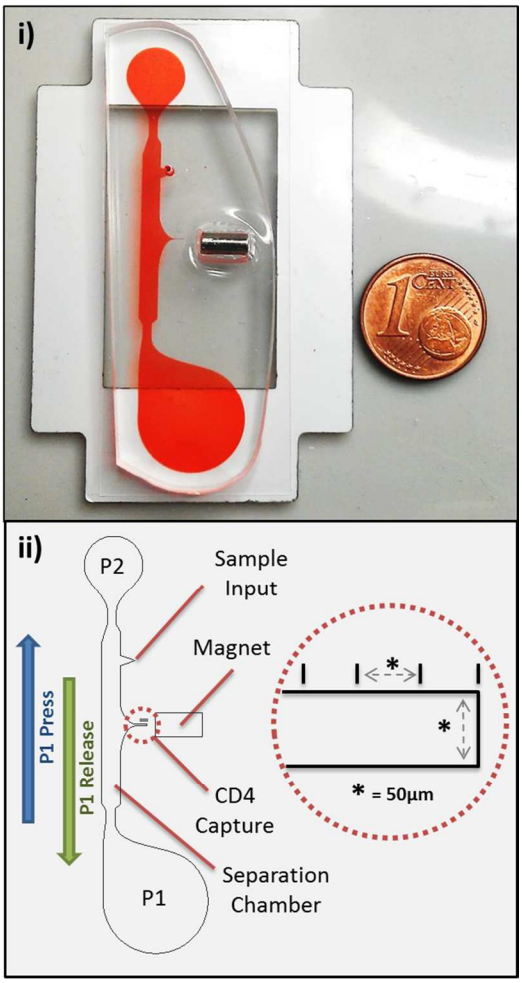

Figure 1: Finger-press actuated magnetophoretic CD4+ isolation chip. i) Image of a chip. The microfluidic structures are highlighted with red dye. ii) Schematic showing main constituents. Direction of flow when P1 is depressed or released is indicated with blue and green arrows, respectively. A zoom of the capture chamber is shown in the circular red insert.

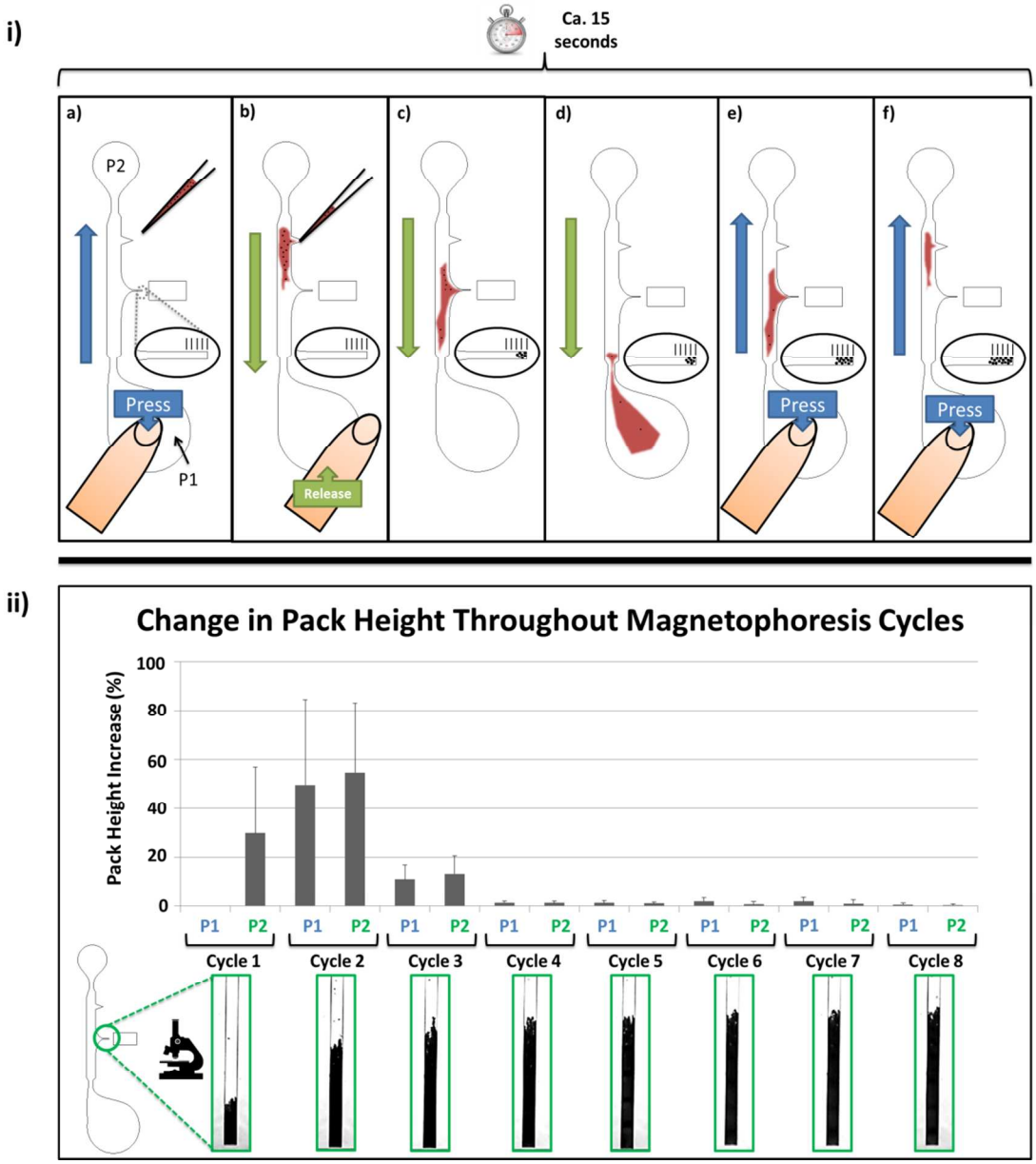

Figure 2: i) Operation of one cycle to isolate CD4+ cells (shown as black circles) from whole blood. Direction of flow pressure is shown with blue (towards P2) and green (towards P1) arrows. Elliptical insert represents a zoomed view of the capture chamber**. ii)** Analysis of the heights of the cell/bead pack in the capture chamber from 1 – 8 cycles. "P1" (blue) and "P2" (Green) indicate the direction of the fluidic force. Images bordered in green represent zoomed micrographs of the capture chamber at the completion of a cycle.

The CD4+ count results from the interplay of two chip-based mechanisms – i) flow-based magnetophoresis, and ii) cell-mediated volume displacement. The execution of the diagnostics protocol involves the following sequence of handling steps. First, the elastic membrane sealing the pneumatic chamber (P1) is depressed (Fig. 2a). Due to the reduction of the internal volume of the chip, a corresponding fraction of liquid is expelled *via* the sample input port and wicked away using an absorbent tissue. 4 µl of sample is then applied to the loading port before the membrane at P1 is released (Fig. 2i a-b). The subsequent reconstitution of the initial internal chip volume generates an underpressure which drives sample from the sample port, past the capture region, and towards reservoir P1 (Fig. 2i c-d). As the volume of displacement resulting from depressing P1 (ca. 6 µl) exceeds that of the applied sample (4 µl), the full sample volume is drawn into the chip upon release of P1. Due to the described volumes, some air can also enter the chip *via* the input port during loading. When small volumes of air enter the chip, P2 provides excess priming liquid to minimise the effect on the fluidic flow.

Due to the small dimensions of the microfluidic structure (the chamber is 40 µm in depth), the finger-actuated, pressure-driven flow through the primary channel connecting P1 and P2 stays in the laminar regime, thus resulting in practically stag-

nant flow in the dead-ended lateral capture region (which would otherwise feature excessive viscous shear due to the close proximity of incoming and outgoing flow lines). Untagged background cells simply follow the streamlines by means of the Stokes drag and are thus barred from the stagnant capture zone (ESI video V.1). Instead this capture zone will be almost exclusively populated by magnetic particles, i.e. free beads and magnetically tagged (target) cells.

During this pressure-driven magnetophoresis through our chip, the background of non-magnetically tagged cells follows the flow towards P1; only the magnetically tagged CD4-positive cells (and any unbound magnetic beads) are deflected towards the base of the flow-free capture chamber (Fig. 3). In order to sequester remaining CD4+ cells to the capture chamber, P1 is again pressed to propel the sample back past the capture chamber and towards the sample input port (Fig. 2i e-f). This dual-press pumping completes within 15 seconds. After three complete dual-press pumping cycles (i.e. six passes of the capture chamber within about 45 seconds), the increase in the height of the cell / bead pack in the capture chamber reaches a plateau; further cycles result in only minimal changes in the observed height (Fig. 2ii). Hence, for data shown in this work, three dual-press pumping cycles were performed unless otherwise stated.

As they possess a diameter of 4.5 ± 0.07 µm, which falls just short of half the average radius of the CD4+ cells (ca. 12 - 15 µm [31]), the magnetic beads are too large to be internalized into the cells. Consequently, to a good approximation, the volumes of cells and beads are additive, leading to a linear relation between the number of CD4+ cells isolated to the capture chamber and the filling level. The slope is governed by the cell size and chamber geometry and can be calibrated with samples exhibiting defined numbers of CD4+ cells. The offset, "zero cell" volume can be quantified with a sample fully depleted of CD4+ cells and spiked with a standard number of magnetic beads.

The filling level (and thus a metric for the concentration of CD4+ cells) can be measured using bright-field microscopy by comparison to a scale alongside the capture chamber – much like reading a thermometer. Alternatively, in particular for validation purposes, cells can be enumerated by fluorescence measurement of stained white blood cells (Figs. 4 - 5). In many similar applications, CD4+ cells are fluorescently detected using specific anti-CD4 fluorescent antibodies as a consumable. However, especially for applications in global diagnostics, the rather high costs of the fluorescently-conjugated antibodies and the necessity of a cold chain shipping and storage (or short shelf-life) can be limiting factors. While the Dynabead™ CD4 magnetic beads used in the presented chip are recommended to be stored at 4-8 °C, they are shipped in liquid form without the need for refrigeration; and the protocols utilising the beads are all carried out at room temperature. Further, the potential costs of a high efficiency reagent such as Dynabead™ CD4 for an assay designed to be low-cost can be offset by the low volume required per test when performed using the microfluidic architectures of the presented chip. Optional antibody-free fluorescent detection is also facilitated through DNA-binding, UV-excited 4',6-diamidino-2-phenylindole (DAPI); a common white blood cell (WBC) stain. As red blood cells do not possess a DNA-containing nucleus, DAPI will stain the entire WBC population, but not the RBCs. Since the diagnostic specificity of our system is not based on the affinity of a specific fluorescent stain to the target cells, but rather on the affinity and relocation of the magnetic beads, the level of CD4+ can be thus measured by the aggregate fluorescence arising from the capture chamber. All other WBCs, while also DAPI-stained, will be located in the segregation channel and disregarded by the observer. This allows a specific CD4+ fluorescent-based measurement (if required) without the expense and difficulties associated with specific biological reagents such as antibodies.

Materials and Methods

Chip Fabrication and Priming

The microfluidic chips were formed from a silicone elastomer – polydimethylsiloxane (PDMS) (Dow Corning, MI, USA); mixed at a ratio of 10:1 base and curing agent. The procedures for making the master mould [32, 33] and the cavities required for securing the on-chip magnets in the PDMS and curing the PDMS in the moulding rig have been described elsewhere [21].

Once the PDMS is cured and the magnetic positioning mould has been removed, the PDMS chips were cut out and pealed from the wafer, leaving 40-µm deep microfluidic structures on the underside, and cavities for placing the magnets through the PDMS. A sample-loading hole was defined in the PDMS using a dot punch. The PDMS slab was placed onto a 25×60 mm^2 glass substrate, and allowed to bond for 30 s. Finally, using pressure sensitive adhesive (PSA – Adhesives Research, Ireland), the PDMS / glass chip was secured to a supporting bracket cut from polymethylmethacrylate (PMMA) (Radionics, Ireland) by a CO2 laser writer (Epilog Zing, USA).

To prime the microchannels, the chips were placed under vacuum for at least 1 hour. Subsequently a large drop of priming buffer (PBS pH 7.4, 0.1% w/v BSA, 1 mM EDTA) was placed on the surface of the PDMS, covering the sample-loading hole. Degas-driven flow then primes the channels [34]. We used NdFeB N45 cylindrical magnets, with a diameter of 3 mm and a height of 6 mm (Supermagnete, Germany). These magnets were placed in the moulded cavities before the sample was loaded to the chip.

Sample Preparation

The operation and efficiency of the chip was tested using three types of input samples. A) The ability of the chip to perform flow-based magnetophoresis was demonstrated using a mixture of magnetic and non-magnetic beads, with the latter being additionally fluorescent. B) Cell-mediated volume displacement was demonstrated using whole blood as starting material, spiked with fluorescently stained HL60 cells. Finally, C) a standard curve of whole blood with increasing numbers of native CD4+ cells was used to demonstrate the chip in its

diagnostic mode. The sample preparation protocols for all these sample types are documented in the electronic supplementary material (ESI).

Microscopic Imaging and Quantification of Signal

Cell / bead packing in the detection chamber was visualised on-chip using an Olympus IX81 inverted epifluorescent microscope (Olympus, Tokyo, Japan). For non-fluorescence quantification, the height of the packing was simply compared by eye to the scale bar integrated alongside the detection chamber (Figs. 4-5) by bright-field microscopy. The result reported by this method represents the notch that the highest event in the capture chamber reaches when viewed visually. If the level is found between two notches, then the higher of the two is reported. For fluorescence-based quantification, we employ DAPI staining of WBCs, or the NucBlue™ staining of spiked HL60 cells – both of which are detected using a UV-excitation filter set on the microscope (Ex = 370 nm, Em = 460 nm). The method for calculating the relative levels of fluorescent signal between samples is described in detail in the ESI.

Experimental Results

Flow-based Magnetophoresis

To demonstrate its capability to isolate magnetically-tagged particles from a background population of non-magnetic particles, a mixture of magnetic and non-magnetic particles was processed on the chip. The particle size in both populations was similar (10 µm – 11 µm), and chosen to approximately mimic the size of target cells. For further distinction only the non-magnetic particles were infused with FITC and so could be detected fluorescently. Suspensions were prepared at a number ratio of 2500 non-magnetic to 500 magnetic particles per µl sample. 4 µl of this sample was loaded to the chip and processed using the three cycles as described in Fig. 2.

Following flow-based magnetophoretic processing of the sample, the majority (93.0 ± 3.3%) of the magnetic particles arrived in the capture chamber where only a small proportion (0.01 ± 0.02%) of the originally abundant fluorescent particles (green) were observed (Fig. 3i-ii). These non-magnetic beads may have been conveyed to the capture zone by either binding to one of the deflected magnetic particles, or by their entrapment in the migration of the magnetic particles. Conversely, 99.99 ± 0.02% of the non-magnetic particles, and 7.0 ± 3.3% of the magnetic particles remained in the separation chamber (Fig. 3ii). Overall, the two populations were efficiently isolated from each other using flow-based magnetophoresis within 45 seconds of sample application to the chip.

Cell-Mediated Volume Displacement

In order to show the effect of a cellular population co-localising with magnetic beads in the capture chamber, both depleted blood and depleted blood supplemented with cultured and NucBlue™ stained HL60 cells were processed on chip (method

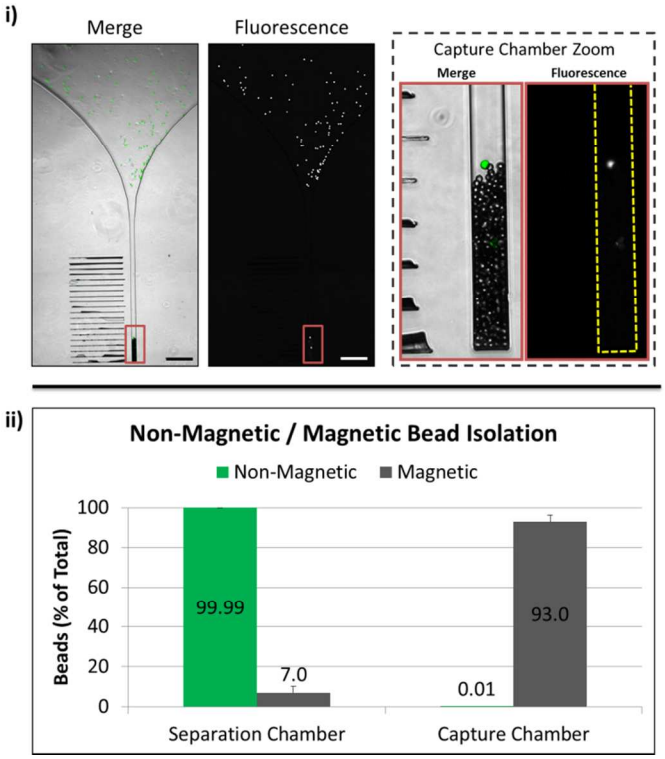

Figure 3: i) Results of finger-press pumped magnetophoretic isolation of 10 µm magnetic beads (black) from 11 µm non-magnetic fluorescent beads (coloured green in the merged images). The areas enclosed by the red boxes are shown magnified on the right. The edge of the capture chamber is shown as a yellow dashed line in the zoomed fluorescent image. Scale bar is 0.5 mm. **ii)** Statistical analysis of the distribution of non-magnetic and magnetic particles. Error bars represent one standard deviation. Data was collected over n=3 experiments.

of blood processing and HL60 staining / spiking is described in supplementary information). In both cases, the same number of Dynabead™ CD4 magnetic beads were added to the samples (ca. 5.1×10^4 µl^{-1}). HL60 cells were added to depleted blood at a concentration of 1600 cells / µl whole blood, thus falling within the medically relevant healthy level of CD4+. Following three of the dual-press pumping cycles described in Fig. 2, the capture chambers were observed by brightfield and fluorescent microscopy.

In the absence of HL60 cells, the level of bead packing in the capture chamber reached a height of 0.23 ± 0.03 mm, corresponding approximately to the mid-point between notch 4 and 5. Since the larger value is used as the diagnostic metric when the pack height lies between two notches, the zero-cell metric is recorded as 5 (Fig. 4i). Accordingly, repeated experiments (n = 4), resulted in a mode of 5 when pack height was measured against the integrated notch scale (Fig. 4ii). When an identical sample is processed supplemented with HL60 cells, the pack height is 0.48 ± 0.04 mm, corresponding to 9 - 10 (mode = 10) on the notch scale (Fig. 4i-ii). The presence of HL60 cells is confirmed using UV fluorescence (note that the CD4 beads do not show auto-fluorescence under UV illumination). Given that the concentration of beads between the two samples are identical, the increase in packing level can

reasonably be assumed to scale with the number of CD4 expressing HL60 cells present.

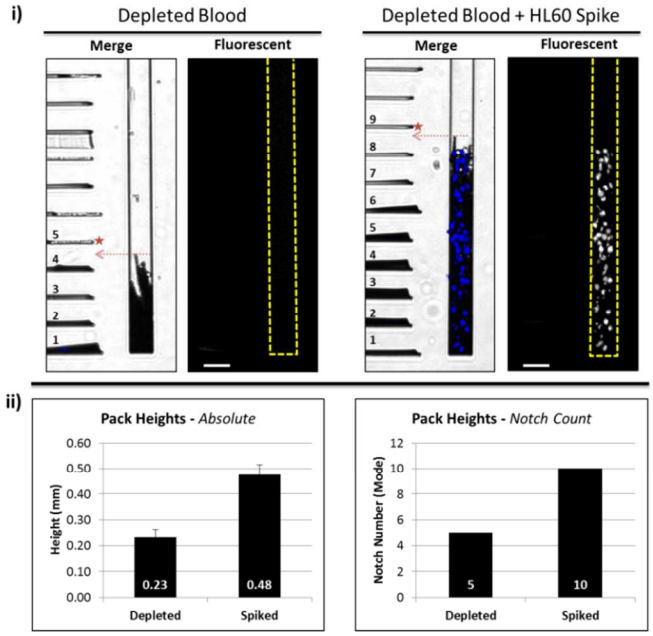

Figure 4: i) Results of finger-press pumped magnetophoretic isolation of fluorescently stained CD4-positive cultured cells (HL60) from whole blood that has been depleted of native CD14 and CD4 cells. HL60 cells were spiked to the depleted blood at 1600 cells / µl to represent a medically relevant concentration. Merged brightfield / fluorescent images are shown on the left, raw fluorescent images are shown on the right. The highest level of bead / cell packing reached is indicated by a red arrow, and the notch corresponding to the associated metric is indicated with a red star. Scale bar is 0.05 mm. **ii)** Statistical analysis of cell-mediated volume displacement. Pack heights are measured as both absolute height (in mm) and the corresponding modal notch number on the integrated scale. Error bars represent one standard deviation, n=4 experiments were carried out.

Native CD4+ Cell Analysis from Whole Blood

The goal of the presented chip is to address the requirement for a diagnostic test for starting ART treatment in patients infected (or suspected infection) with HIV. HL60 cells are CD4 positive and can hence be employed to demonstrate the functionality of the chip (Fig. 4); however, as these are cultured cells, they may not be representative of native blood-borne cells with regard to size – and thus one cannot base a diagnostic standard curve on HL60 cells. To address this without the need to resort to bio-hazardous blood from HIV-positive individuals, we generated real blood samples with adjustable numbers of target cells by mixing blood fully depleted of CD4+ with blood populated with a given number of CD4+ cells (Fig. S.1). To rule out issues with type-based coagulation, both samples originated from the same donor. Using this strategy, a number of samples covering the range of CD4+ concentrations in a diagnostically relevant range were prepared and processed as described.

The upper level of the bead / cell packing increases with the number / concentration of CD4+ cells. Below the current WHO threshold for ART initiation (500 CD4+ cells / µl), the level is in the range of 5-7 notches on the integrated scale (Fig. 5). At the lower levels of CD4+ concentration, there can be slightly

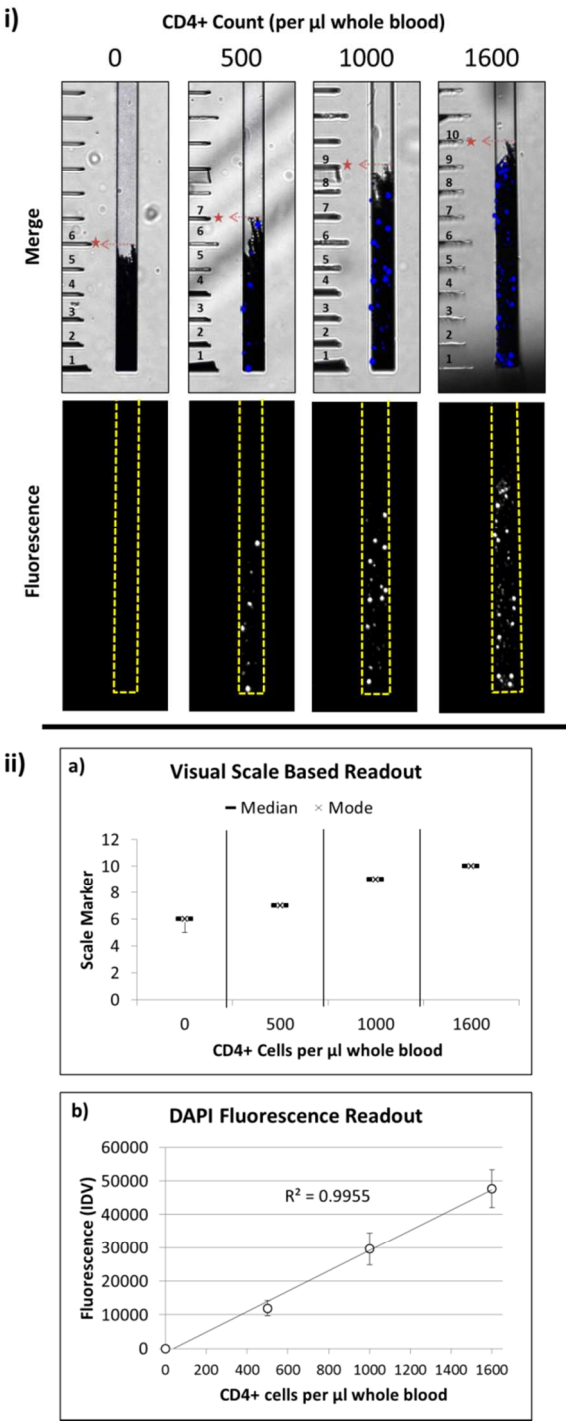

Figure 5: i) Results of finger-press pumped magnetophoretic isolation of native CD4+ cells from whole blood. Samples were prepared by mixing fully CD4+ depleted blood with non-depleted blood to achieve the CD4+ concentrations indicated. Fluorescent signal is generated by incubation of whole blood with DAPI during sample preparation. **ii)** Analysis was based on simple observation of the upper level of packing compared to the integrated visual scale alongside the capture chamber, and also by DAPI-based fluorescence. (a) Visual readout analysis - upper and lower bars represent the maximum and minimum reading, respectively; the median and mode readings are also displayed. (b) Fluorescent analysis - the integrated density values (IDV) from identically sized ROIs from the images were calculated relative to the number of native CD4+ cells in the original blood sample. Error bars represent one standard deviation. In both (a) and (b), data was collected over n = 4 experiments.

variable results linked to the secondary bead structures that tend to form around the magnetic field lines at the top of the bead / cell pack. This is possibly due to the elevated excess of unbound beads in the pack at lower cell concentrations. Such artefacts can be clearly discerned in the upper part of the 500 CD4+ per µl images in Fig. S.2 (ESI). As the metric is based on the highest point of the pack, such a secondary structure may lead to slight fluctuation in the recorded result. The level is more stable between experiments as the CD4+ concentration rises into the healthy ranges (>1000 cells / µl). This observation highlights that although the result can to a limited degree be subjective to the observer, bright-field observation can yet be utilised to identify samples in the lower CD4+ range without the need of equipment more complex than a low-end magnification device.

Given that a known number of beads is added to a sample, and the volume of a bead population can be calculated based on the low variation in bead size (± 1.5%) - the volume the bead pack theoretically occupies can hence be estimated (Fig. S.3). When compared to the actual volume occupied by a bead pack in the absence of target cells, the observed packing volume is significantly lower than expected (Fig. S.3). It is unknown why this discrepancy exists; however, the extent of the error produced appears to be consistent as demonstrated by the repeatable experimental results observed (Figs 4 – 5). Thus, although of interest for further investigation, the discrepancy does not significantly hamper the diagnostic use of the chip.

Using dark-field fluorescence measurement of the capture chamber when sample preparation was performed in the presence of DAPI, we recorded a linear relationship between fluorescent signal and cell concentration (Fig. 5ii-b). As an improvement to the bright-field results, the data across experiments groups tighter around the lower CD4+ levels than the higher levels using the fluorescence based method. These data suggest that a first level of screening could be carried out using rapid and equipment-free bright-field observation to identify individuals with healthy levels of CD4+ cells in the blood (for example, with a result of ≥ 8 notches). Individuals presenting with a brightfield result below 8 notches could then have the same test chip analysed by a simple optical instrument capable of UV-illumination to determine more accurate low-range CD4+ estimations, without the need to re-sample the blood.

Summary & Outlook

In summary, we present a microfluidic, dual-force device, incorporating regions of flow and stagnant conditions, for the isolation and numerical estimation of the HIV-relevant CD4+ cell type from a patient's blood sample. Instrument-free operation is enabled by finger-press actuated pumping in combination with magnetophoretic separation through a conventional magnet which can readily be re-used. We successfully demonstrated high capture efficiency of magnetic events from a background of non-magnetic particles. A linear relationship was observed between the concentration of CD4+ cells harboured in blood and the packing level detected in the capture region. This endpoint can be queried by two methods – bright-field magnification and fluorescence output. In the case of the fluorescence method, no specific antibody reagent is required – thereby reducing the cost-per-test of the chip.

This work represents a significant advancement towards a CD4+ counting PoC device commensurate with the very challenging techno-economical demands in resource-poor settings where HIV/AIDS is endemic. Future work will focus on incorporating the few, still off-chip preparation steps into the chip, facilitating the entirety of the diagnostic to be processed locally, and driven by finger-pumping.

Acknowledgements

This work was supported by Enterprise Ireland (Grant No CF 2011 1317) and the Science Foundation Ireland (Grant No 10/CE/B1821).

Notes and references

Biomedical Diagnostics Institute, National Centre for Sensor Research, School of Physical Sciences, Dublin City University, Ireland.
Email: jens.ducree@dcu.ie **or** macdara.glynn@dcu.ie

Electronic Supplementary Information (ESI) available: [ESI Document: S.1 Sample Preparation, S.2 Optional Fluorescent Imaging and Quantification of Signal, S.3 Supplementary Experimental Results, S.4 Packing Volume Analysis; ESI Video: V.1 Stagnant flow in capture chamber]. See DOI: 10.1039/b000000x/

1 F. Barré-Sinoussi, J. C. Chermann, F. Rey, M. T. Nugeyre, S. Chamaret, J. Gruest, C. Dauguet, C. Axler-Blin, F. Vézinet-Brun and C. Rouzioux, *Science,* 1983, **220**, 868-871 (DOI:10.1126/science.6189183).

2 R. C. Gallo, P. S. Sarin, E. Gelmann, M. Robert-Guroff, E. Richardson, V. Kalyanaraman, D. Mann, G. D. Sidhu, R. E. Stahl and S. Zolla-Pazner, *Science,* 1983, **220**, 865-867 (DOI:10.1126/science.6601823).

3 UNAIDS, *Global report: UNAIDS report on the global AIDS epidemic 2013*, UNAIDS / JC2502/1/E, WHO, Geneva, 2013.

4 J. Bor, A. J. Herbst, M. Newell and T. Bärnighausen, *Science,* 2013, **339**, 961-965 (DOI:10.1126/science.1230413).

5 M. J. Mugavero, K. R. Amico, T. Horn and M. A. Thompson, *Clin. Infect. Dis.,* 2013, **57**, 1164-1171 (DOI:10.1093/cid/cit420 [doi]).

6 E. M. Gardner, M. P. McLees, J. F. Steiner, C. Del Rio and W. J. Burman, *Clin. Infect. Dis.,* 2011, **52**, 793-800 (DOI:10.1093/cid/ciq243 [doi]).

7 S. Rosen and M. P. Fox, *PLoS Medicine,* 2011, **8**, e1001056 (DOI:10.1371/journal.pmed.1001056).

8 E. Losina, I. V. Bassett, J. Giddy, S. Chetty, S. Regan, R. P. Walensky, D. Ross, C. A. Scott, L. M. Uhler and J. N. Katz, *PLoS One,* 2010, **5**, e9538 (DOI:10.1371/journal.pone.0009538).

9 C. D. Chin, T. Laksanasopin, Y. K. Cheung, D. Steinmiller, V. Linder, H. Parsa, J. Wang, H. Moore, R. Rouse and G. Umviligihozo, *Nat. Med.,* 2011, **17**, 1015-1019 (DOI:10.1038/nm.2408).

10 I. V. Jani, N. E. Sitoe, E. R. Alfai, P. L. Chongo, J. I. Quevedo, B. M. Rocha, J. D. Lehe and T. F. Peter, *Lancet,* 2011, **378**, 1572-1579 (DOI:10.1016/S0140- 6736(11)61052-0).

11 M. T. Glynn, D. Kinahan and J. Ducree, *Lab Chip,* 2013, (DOI:10.1039/C3LC50213A).

12 C. Mair, S. Hawes, H. Agne, P. Sow, I. N'doye, L. Manhart, P. Fu, G. Gottlieb and N. Kiviat, *Clin. Exp. Immunol.,* 2008, **151**, 432-440 (DOI:10.1111/j.1365-2249.2007.03573.x).

13 A. Yaman, S. Çetiner, F. Kibar, Y. Tasova, G. Seydaoglu and I. H. Dündar, *Med. Princ. Pract.,* 2005, **14**, 189-193 (DOI:10.1159/000084638).

14 X. Qiu, J. A. Thompson, Z. Chen, C. Liu, D. Chen, S. Ramprasad, M. G. Mauk, S. Ongagna, C. Barber and W. R. Abrams, *Biomed. Microdevices,* 2009, **11**, 1175-1186 (DOI:10.1007/s10544-009-9334-4).

15 K. Xu, M. Begley and J. Landers, *microTAS,* 2013, , 654-656.

16 N. L. Jeon, D. T. Chiu, C. J. Wargo, H. Wu, I. S. Choi, J. R. Anderson and G. M. Whitesides, *Biomed. Microdevices,* 2002, **4**, 117-121 (DOI:10.1023/A:1014683114796).

17 J. Moorthy, G. A. Mensing, D. Kim, S. Mohanty, D. T. Eddington, W. H. Tepp, E. A. Johnson and D. J. Beebe, *Electrophoresis,* 2004, **25**, 1705-1713 (DOI:10.1002/elps.200405888).

18 W. Li, T. Chen, Z. Chen, P. Fei, Z. Yu, Y. Pang and Y. Huang, *Lab Chip,* 2012, **12**, 1587-1590 (DOI:10.1039/C2LC40125H).

19 W. Chang, H. Shang, R. M. Perera, S. Lok, D. Sedlak, R. J. Kuhn and G. U. Lee, *Analyst,* 2008, **133**, 233-240 (DOI:10.1039/b710997k).

20 N. Pamme and C. Wilhelm, *Lab Chip,* 2006, **6**, 974-980 (DOI:10.1039/B604542A).

21 M. Glynn, D. Kirby, D. Chung, D. J. Kinahan, G. Kijanka and J. Ducree, *J. Lab. Autom.,* 2013, (DOI:10.1177/2211068213504759).

22 X. Cheng, D. Irimia, M. Dixon, K. Sekine, U. Demirci, L. Zamir, R. G. Tompkins, W. Rodriguez and M. Toner, *Lab Chip,* 2007, **7**, 170-178 (DOI:10.1039/B612966H).

23 S. Thorslund, R. Larsson, F. Nikolajeff, J. Bergquist and J. Sanchez, *Sensors Actuators B: Chem.,* 2007, **123**, 847-855 (DOI:10.1016/j.snb.2006.10.034).

24 A. Ymeti, X. Li, B. Lunter, C. Breukers, A. G. J. Tibbe, L. W. M. M. Terstappen and J. Greve, *Cytometry Part A,* 2007, **71A**, 132-142 (DOI:10.1002/cyto.a.20375).

25 X. Li, C. Breukers, A. Ymeti, B. Lunter, L. W. M. M. Terstappen and J. Greve, *Cytometry Part B: Clinical Cytometry,* 2009, **76B**, 118-126 (DOI:10.1002/cyto.b.20445).

26 N. N. Watkins, S. Sridhar, X. Cheng, G. D. Chen, M. Toner, W. Rodriguez and R. Bashir, *Lab Chip,* 2011, **11**, 1437-1447 (DOI:10.1039/C0LC00556H).

27 N. N. Mishra, S. Retterer, T. J. Zieziulewicz, M. Isaacson, D. Szarowski, D. E. Mousseau, D. A. Lawrence and J. N. Turner, *Biosensors and Bioelectronics,* 2005, **21**, 696-704 (DOI:10.1016/j.bios.2005.01.011).

28 X. Jiang and M. G. Spencer, *Biosensors and Bioelectronics,* 2010, **25**, 1622-1628 (DOI:10.1016/j.bios.2009.11.024).

29 G. Stybayeva, M. Kairova, E. Ramanculov, A. L. Simonian and A. Revzin, *Colloids and Surfaces B: Biointerfaces,* 2010, **80**, 251-255 (DOI:10.1016/j.colsurfb.2010.06.015).

30 S. Moon, H. O. Keles, A. Ozcan, A. Khademhosseini, E. Hæggstrom, D. Kuritzkes and U. Demirci, *Biosensors and Bioelectronics,* 2009, **24**, 3208-3214 (DOI:10.1016/j.bios.2009.03.037).

31 P. R. Wheater, H. G. Burkitt and V. G. Daniels, *Functional histology. A text and colour atlas.*, Churchill Livingstone, Edinburgh, 1979.

32 D. Kirby, J. Siegrist, G. Kijanka, L. Zavattoni, O. Sheils, J. O'Leary, R. Burger and J. Ducrée, *Microfluid Nanofluid,* 2012, , 1-10 (DOI:10.1007/s10404-012-1007-6).

33 R. Burger, P. Reith, G. Kijanka, V. Akujobi, P. Abgrall and J. Ducrée, *Lab Chip,* 2012, **12**, 1289-1295 (DOI:129510.1039/C2LC21170J).

34 K. Hosokawa, K. Sato, N. Ichikawa and M. Maeda, *Lab Chip,* 2004, **4**, 181-185 (DOI:10.1039/B403930K).

